Journal of Materials Chemistry A

Accepted Manuscript

ROYAL SOCIETY OF CHEMISTRY

www.rsc.org/materialsA

Cite this: DOI: 10.1039/c0xx00000x

www.rsc.org/xxxxxx

ARTICLE TYPE

Precursor-directed synthesis of well-facetted brookite TiO_2 single crystals for efficient photocatalytic performances

Yangsen Xu, Haifeng Lin, Liping Li*, Xinsong Huang, and Guangshe Li*

Received (in XXX, XXX) Xth XXXXXXXXX 20XX, Accepted Xth XXXXXXXXX 20XX

DOI: 10.1039/b000000x

Brookite-TiO_2 is a promising next-generation semiconductor material for solar energy conversion, but it suffers from the difficulty in achieving high quality and phase purity due to its metastable characteristic. Long-chain fatty acid modification or surfactant assisted methods could orient the growth of brookite, however, purifying the products is complicated and the surface reactivity is invariably undermined. Here, we demonstrate the design and tuneable synthesis of brookite nanostructures with geometric features of quasi-octahedral (QO), ellipsoid-tipped (ET) and wedge-tipped (WT) nanorods exposed primarily with {210} facet via water-soluble titanium precursors. When tested as a photocatalyst for hydrogen evolution from water or degradation of organic pollutant, QO brookite nanocrystals showed the highest catalytic activity when comparing to ET and WT nanorods counterparts. This observation could be due to the redox facets that formed "surface-heterojunction" and promoted the separation of the photogenerated carries. The precursor-directed method reported here may usher a new phase for the synthesis of novel metastable nanocrystals with specific facet exposure that are highly useful for applications in energy conversion and environment protection.

1. Introduction

Polymorphs of TiO_2, with the compositions that are abundant in Earth's crust have shown great impacts on a wide range of scientific inquiries and technological applications for its chemical activity, environmental benign and low cost.[1, 2] Three most common polymorphs like rutile, anatase and brookite are built by the same fundamental TiO_6 polyhedral units, while the phase formation differs only due to the nature of connection fashion (sharing corners or edges). Brookite, previously treated as the least studied TiO_2 phase,[3] has drawn an increasing interest recently in pure phase preparation and applications in environmental and energetic fields.[4-7]

Brookite is also a representative metastable phase. Its TiO_6 polyhedral units in orthorhombic structure (space group: P_{bca}) share three edges and corners of octahedron, and arrange parallel to *c*-axis, forming chains with edge sharing and then cross-linked via the shared edges. These features totally differ from those of tetragonal structures of rutile and anatase counterparts that are organized in terms of shared faces.[8, 9] In addition, the arrangement of distorted TiO_6 octahedra is similar for all these polymorphs, which makes it difficult to obtain brookite in pure-phase. As a result, one could usually observe brookite as a by-product of anatase or rutile.[10, 11] Therefore, high-quality metastable brookite crystals have to be obtained just by deliberate control at atomic scale over TiO_6 octahedral configurations. Although a multitude of efforts have been devoted in this regard, it is still a challenge to simultaneously control the structure and high quality brookite. For instance, brookite nanorods[12] and nanotubes[13] have been prepared by an inorganic sodium titanate $Na_xH_{2-x}Ti_3O_7{\cdot}nH_2O$ precursor. Meanwhile, it has been considered that Na^+ ions and basic environment are essential for the formation of pure brookite by hydrothermal conditions.[14, 15] Several cations can initially serve as the stabilizers for the layered structure of lepidocrocite titanate, an intermediate that could transform to the single crystalline brookite.[16] Even so, using these methods, one cannot achieve well crystlline brookite nanocrystals with well-facetted or specific facets exposed, essential for property tailoring.

Precursor-directed approaches based on inorganic-organic hybrid compounds have been deemed as an effective way to achieve various functional inorganic nanomaterials with unique composition, morphology and size.[17-19] Concerning the synthesis of brookite TiO_2, water-soluble titanium complexes have been proved promising in constructing high quality nanoparticles.[20, 21] Ellipsoid-like brookite with a high crystallinity has been prepared by an intermediate with the ligands of oxalate anions in the form of $Ti_2O_3(H_2O)_2(C_2O_4){\cdot}H_2O$.[5] Other shapes like nanorods and nanosheets were also prepared by forming an organic-inorganic titanium compound with glycolic acid, $(NH_4)_6[Ti_4(C_2H_2O_3)_4(C_2H_3O_3)_2(O_2)_4O_2]{\cdot}4H_2O$ in a monoclinic structure (space group: $P_{21/n}$).[20, 22] An oleate-modified hydrothermal growth process can further turn the shape of brookite nanocrystals from rod morphology to pseudo-cube shape which exposed mainly with four {210} and two {001} faces.[23] Recently, our group developed a novel in situ-generated precursor, $[Ti(C_3H_4O_3)_3]^{2-}$ or $Na_2Ti(C_3H_4O_3)_3$, that has yielded high-quality brookite TiO_2 nanosheets and nanorods surrounded with four {210}, two {101} and {201} facets through a low-basicity hydrothermal process.[6, 24] Such a precursor method does not follow the rules previously claimed. For the latter case, crystalline brookite should be obtained in the presence of lots of Cl^-.[25] Kandiel et al.[26] used a commercially available water-soluble titanium bis(ammonium lactate) dihydroxide (TALH) as a precursor and synthesized high quality brookite nanorods with the

exposure of (210) and (111) facets, which is also the only example that the intensity of (211) diffraction located at two theta of 30.81°is higher than (210) peak at 25.3° in the ever reported brookite TiO_2. Hierarchical metastable brookite microsphere has been reported by hydrothermal treatment of water-soluble titanium-picolinato complex in alkaline solution (pH=10).[27] A surfactant-assisted nonaqueous strategy, relying on high-temperature aminolysis of titanium carboxylate complexes, has been developed to anisotropically shaped TiO_2 nanocrystals growing along the [001] direction.[28] However, this synthetic strategy involves extremely complicated procedures or capping complexes that invariably undermine the surface reactivity. Thus, water-soluble complexes of titanium are believed to be the encouraging reagents for the preparation of metastable single phase brookite TiO_2.

Based on these previous studies, the main incentive of this work is to broaden the synthetic condition range for different shapes of brookite by controlling the terminal faces of the single crystal brookite TiO_2. Herein, we report on a selective synthesis of quasi-octahedral nanocrystal, ellipsoid-tipped and wedge-tipped brookite TiO_2 nanorods with available and low toxic ligands by tuning the hydrothermal treatment procedures. Furthermore, the achieved brookite quasi-octahedral nanocrystals with exposure of reductive facets could orient the deposition of noble metals, leading to an excellent photocatalytic property toward hydrogen generation from water and organic pollutant degradation. Atomic configuration of the exposed facets and the mechanism about the transformation of photoexcited holes and electrons were also proposed.

2. Experimental

2.1 Sample Synthesis

All chemicals were purchased from Sinopharm Chemical Reagent Corp, P. R. China and used without further purification.

Brookite ellipsoid-tipped (ET) nanorods. In a conventional operation, under agitating conditions, 0.015 mol $TiOSO_4{\cdot}2H_2O$ was added into 60 mL deionized water as held by a Teflon autoclave to yield a white suspension. Subsequently, 0.25 mol urea and 0.032 mol sodium glycolate were solubilized in turn to generate a yellowish solution. The autoclave was then sealed and kept in an oven at 200 ℃ for 24 h to obtain precipitates. The resultant white precipitates were washed with deionized water and ethanol and dried at 80 ℃ to get ET nanorods.

Brookite wedge-tipped (WT) nanorods. Typically, a strong acidic titanium- contained solution of 0.25 M was prepared beforehand by slowly dropping $TiCl_4$ into the ice-cooled deionized water. Afterwards, 0.25 mol urea and 5 mL sodium lactate solution (60 %) were mingled into 60 mL of the above acidic solution with agitation, respectively. Finally, the solution was reacted hydrothermally at 200 ℃ for 12 h. After reaction, the product was washed and dried at 80 ℃.

Brookite quasi-octahedral nanocrystals. The fabrication of quasi-octahedral nanocrystal was done according to the processes employed for synthesizing WT nanorods but with a notably declined supply (0.083 mol) of in-situ alkali source, i.e. urea, to slow down the formation of monomers deriving from decompose of water-soluble titanium-involved complexes.

2.2 Sample Characterization

X-ray diffraction (XRD) patterns of the samples were collected by a Rigaku MiniFlex II diffractometer (Cu Kα radiation) at 30 kV and 15 mA. Transmission electron microscopy (TEM) and high-resolution transmission electron microscopy (HRTEM) were placed in a Tecnai G2 F20 transmission electron microscope. Raman vibrations of the samples were observed on a Renishaw, UV-vis Raman System 1000 with an excitation light of 532 nm. UV-vis diffuse reflectance spectra of the samples were recorded with a Varian Cary 500 UV-vis-NIR spectrometer. Brunauer-Emmett-Teller (BET) specific surface areas were tested using a Micromeritics ASAP 2020 system. Chemical compositions and valence-band spectra of the samples were examined by X-ray photoelectron spectroscopy (XPS) on an ESCA-LAB MKII apparatus equipped with a monochromatic Al Kα X-ray source.

2.3 Photocatalytic activity measurements

2.3.1 Methyl orange (MO) degradation

The photocatalytic degradation of MO was measured under UV-light illumination (780≥λ≥340 nm). A 300 W Xe lamp with a 340 nm cutoff filter was employed to ensure the desired illuminations, and 100 mL of MO solution (10 mg/L) containing 0.1 g of catalyst was used for the reaction. Before irradiation, MO suspensions with varying catalysts were stirred for 5 h to reach the adsorption and desorption equilibrium. At a regular time interval, the illuminated suspension was extracted and centrifuged at a rate of 9000 rpm to achieve a solid/liquid separation, and the relative content of MO in the supernatant was determined from the UV-vis adsorption spectra, as recorded by a PerKin-Elmer UV lambda 35 spectrophotometer.

2.3.2 Hydrogen evolution

The photocatalytic reaction for hydrogen generation from water was carried out in a 100 mL Pyrex flask with a 300 W Xe lamp equipped with a cutoff filter (780≥λ≥340 nm) as the light source. The reaction temperature was kept at 5 ℃. Typically, 50 mg TiO_2 was dispersed into 80 mL aqueous solution containing 25 vol% methanol filled in the flask, and a H_2PtCl_6 solution acts as co-catalyst was mixed into the suspension to ensure the catalyst a Pt loading of 5 wt%. Before light irradiation, the reactor was sealed, and the residual air was evacuated by a vacuum pump. The experimental duration was set as 4 hours, and the produced gas was detected every 1 hour by a gas chromatograph (Fuli 9790Ⅱ, Zhejiang, China) using TCD detector.

2.4 Photoelectrochemical measurements

The photocurrent detection was performed on a conventional electrochemical cell with a working electrode, a platinum foil counter electrode, and an Ag/AgCl reference electrode. Prior to the test, indium-tin oxide (ITO) conducing glass was ultrasonically cleaned by deionized water, acetone and ethanol for 10 min, respectively. 20 mg TiO_2 were first dispersed into 0.2 mL dimethylformamide under sonication for 1 h to get a slurry, which was then spread onto ITO glass surface to form a 0.5 cm x 0.5 cm film area. Subsequently, the naked part of ITO glass was

coated by epoxy resin. The electrolyte was 0.2 M $NaSO_4$ solution, and the required irradiation was obtained employing a 300 W xenon lamp equipped with a 365 ± 15 nm band pass filter.

3. Results and Discussion

3.1 Crystal phase, microstructure, and formation mechanism of brookite with different shapes

Table 1. Preparation conditions and physicochemical properties of the as-prepared TiO_2

sample \ properties	Urea, mol	ligand [a]	Crystal size [b], nm: length	Crystal size [b], nm: width	BET [c], m^2g^{-1}	P_{210} [d]	I^{211}/I^{210} [e]	E_g, eV	k [f], min^{-1}
ET nanorods	0.25	glycolate	52-75	27±2	34.2	80%	0.97	3.24	0.0078
WT nanorods	0.25	lactate	74±4	21±1	46.5	90%	0.92	3.28	0.0205
quasi-octahedra	0.083	lactate	50-65	40-50	19.8	70%	0.96	3.26	0.0306

Noted: Ligands used are sodium glycolate or sodium lactate. Crystal sizes are statistic data from TEM observations. P_{210} means percentage of {210} planes. I^{211}/I^{210} means the diffractive peak intensity ratio of (211) at two theta of 30.83° to (210) at two theta of 25.36°. k means the apparent reaction rate constant of MO photodegradation, which is calculated based on a pseudo-first-order kinetic model.

A possible formation process of brookite TiO_2 was schematically proposed in Scheme 1. It is noted that the structure (d) in Scheme 1 is a supposed intermediate, which could be vividly shown as the chain-like distorted TiO_6 octahedra building units shared corners and edges in bulk brookite. The water-soluble precursors in this process, actually, involved two complexes: one is $[Ti(OH)_2(H_2O)_4]^{2+}$ octahedron[24] formed when $TiCl_4$ was added into water, as shown in Scheme 1b. With the introduction of sodium lactate, taking WT nanorod for example, the other precursor of titanium-contained complex $[Ti(C_3H_4O_3)_3]^{2-}$ (Scheme 1c) was generated via an analogously ligand exchange reactions. The formations of these brookite precursors have been represented by the reaction equations (1-4) in the supporting information. Under hydrothermal condition and weak base environment, $[Ti(C_3H_4O_3)_3]^{2-}$ may lose a peroxo group, the same as the compound of titanium and glycolic acid,[20] yield a dimer, and then tetramer by a bridging oxo group and further grow to produce stripes of $Ti_{4n}O_{14n+4}$ and finally crystallized to brookite TiO_2 (Scheme 1e).

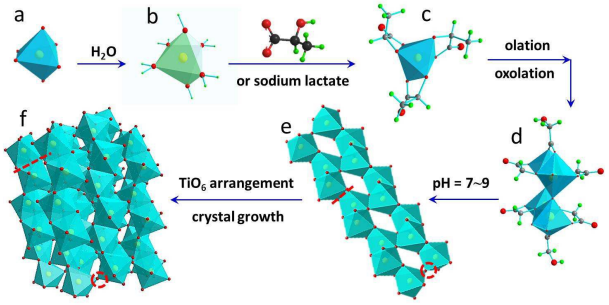

Scheme 1. Formation mechanism proposed for phase-pure brookite TiO_2 via water soluble precursor: (a) TiO_6 octahedra, (b) $[Ti(OH)_2(H_2O)_4]^{2+}$ complex, (c) water soluble $[Ti(C_3H_4O_3)_3]^{2-}$ precursor, (d) possible intermediate of condensed four TiO_6 octahedra, (e) chain-like distorted TiO_6 octahedra which are arranged parallel to *c*-axis in bulk brookite, and (f) bulk structures of brookite, the dashed red circles and lines in (e) and (f) show the shared corners and edges of TiO_6 octahedra.

Following such a process, three morphologies of single phase brookite with high quality were prepared. Table 1 shows the summary of physicochemical properties of the synthesized well-faceted brookite, including quasi-octahedral (QO) nanocrystals, ellipsoid-tipped (ET) and wedge-tipped (WT) nanorods. The pure phase of the as-obtained brookite TiO_2 was proven by X-ray diffraction (XRD) measurements (Fig.S1). The diffraction peaks of each sample match well those of standard diffraction data of brookite (JCPDS NO. 76-1934). The intensity ratios of diffraction {211} at two theta of 30.83° to {210} at 25.36° ($I^{(211)}_{brookite}/I^{(210)}_{brookite}$), which was previously used to identify the phase purity of brookite, are all larger than the standard diffraction data of brookite (about 0.9, as listed in Table 1), which demonstrates that the synthesized TiO_2 is highly crystalline and phase pure. The Raman spectroscopy, a phase-sensitive technique, as described in Fig. S2, further confirms the pure brookite phase. The locations of vibration bands are similar for all three as-prepared brookite samples as to those reported elsewhere.[26]

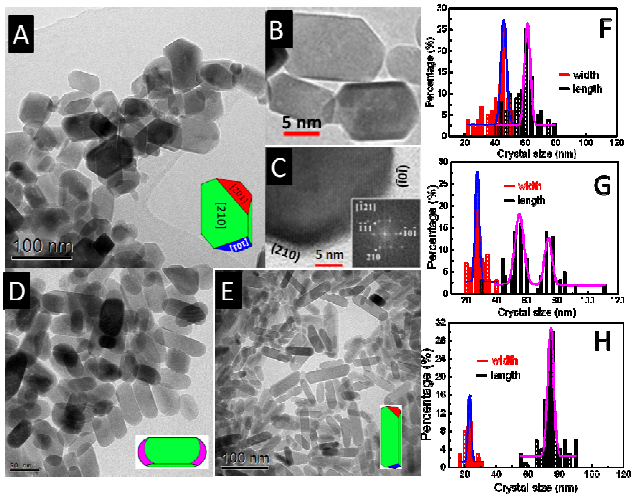

Fig. 1 TEM (A) and HRTEM (B,C) images of the synthesized brookite QO nanocrystals. Inset in (C) is the FFT pattern of QO nanocrystals, (D) and (E) are the TEM images of brookite ET nanorods and WT nanorods, respectively. Insets in (A), (D) and (E) are the schematic diagram of the corresponding brookite nanocrystals with different exposure facets, (F-H) particles size (width and length) distributions of QO nanoparticles, ET and WT nanorods brookite.

TEM and HRTEM images of the well-crystallized brookite exposed with different facets are displayed in Figs. 1 and S3. Fig. 1A presents the obtained QO TiO_2. Close-up view indicates that the average particle width and length for QO were around 45 and 60 nm, respectively (Fig.1B). FFT analysis in Fig. 1C further reveals that the QO particles were dominantly exposed with (210) and (101) facets. Similarly, the average dimensions of brookite ET and WT nanorods were bigger than QO in length and smaller in width, respectively, as displayed in Figs. 1(C, D) and S3 (B, D). More details can be clearly seen from the particles size (width and length) distributions in Figs. 1(F-H). From above observations, it can be found that all these brookite particles were enclosed by four equivalent {210} facets [(210), ($\bar{2}10$), ($2\bar{1}0$) and ($\bar{2}\bar{1}0$)] at the centre part. In addition, the strong diffraction spots in Figs. S3A and S3F demonstrate that QO TiO_2 and WT nanorods are single-crystals. The co-existence of diffraction rings and spots in ET nanorods indicates a complex of single crystal

and polycrtstal (Fig. S3C). The presence of dominant exposed {210} planes could be due to the fact that these facets are the most stable faces and that during the synthesis, the solution or ligand molecules absorbed onto the surface active sites (Ti^{4+} or noncovalent bonding oxygen atoms) in these planes thus may direct the growth of brookite crystals.[20, 23, 28, 29] Two ends of ET nanorods are dominated by curved surface with no specific planes exposed (Figs. 1C and S3C). Interestingly, both ends of QO nanocrystals and WT nanorods are surrounded by {201} and {101} crystal faces (see the schematic diagrams in Fig. 1), and the lattice fringes of the nanorods terminate sharply at two {101} edges and two {201} borders in the [121] zone axis, and [132] crystalline axis, respectively (Figs. S3E, S3F). Further, the percentages of {101} and {201} of QO nanocrystal were both optimized at 15%, which is much larger than those of WT nanorods.

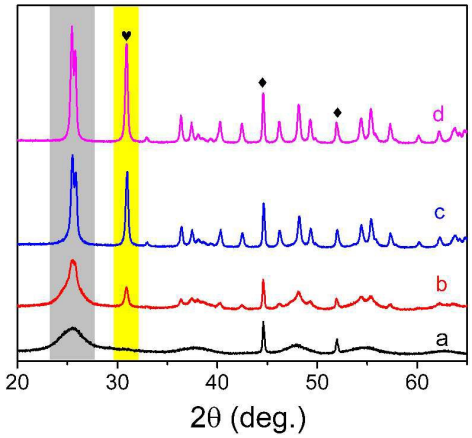

Fig. 2 XRD patterns of the samples synthesized by hydrothermal conditions at 200 ºC for different periods of reaction time: (a) 1 h, (b) 2 h, (c) 5 h, and (d) 12 h. The symbols ♦ and ♥ represent the Bragg peaks of the Ni and the characteristic diffraction peak (211) of brooktie TiO_2, respectively.

The evolution of the phase structure of the obtained products was monitored by XRD based on a batch of time-regulated experiments. As indicated in Fig. 2, the initial solution was highly acidic at a pH value around 1-2, which was gradually increased 7-8 due to the decomposition of urea as the reaction lasted for about 1 h. Anatase TiO_2 with a quite small size (ca. 4 nm as estimated from Scherrer formula) was produced as evidenced by the distinct peak broadening (Fig. 2a). Interestingly, notable orthorhombic brookite TiO_2 (JCPDS No. 76-1934) of about 24 nm appeared when the reaction was proceeded for a duration time of 2 h (pH = 8-9), which can be identified by the newly appeared characteristic diffraction located at $2\theta=30.8^o$ that does not overlap with that for anatase or rutile components in Fig. 2b, as reported elsewhere.[15, 26] Prolonging the preparation time to 5 h (pH = 8-9), XRD signal changed obviously, and the pattern was almost neat brookite (ca. 32 nm) with the elimination of broadened peaks of anatase (Fig. 2a). When the hydrothermal reactions were further sustained to 12 h (pH = 8-9 were applied for all these three circumstances), as indicated in Fig. 2d, the purity of brookite was continuously enhanced, and a single-phase brookite lattice was obtained. Additionally, it has been proved that anatase preferred to exist in highly acidic environment (pH<3), and the structural similarity and high pH (≥8) trigger the phase transformation from anatase to brookite.[15, 26, 28]

It is well documented that morphologies of semiconductors affect the light absorbance and band-gap energies.[24] Uv-vis absorption spectra of diversely shaped brookite crystals are exhibited in Fig. 3. The optical absorption edges were determined to be 378 nm for ET nanorods, 374 nm for WT nanorods, 376 nm for QO nanocrystal and 405 nm for Degussa P25. The band gap (E_g) of these nanocrystals can be fixed according to the relational expression: $A = K(h\nu - E_g)^n/h\nu$, where A is the absorbance, K is a constant, and n can equal 1/2 or 2, which stands separately for the direct transition or indirect transition.[30] Brookite TiO_2 is widely acknowledged as an indirect semiconductor, i. e. n=2 (ref[8]). The optical band gap energy of these TiO_2 samples was calculated to be 3.24 eV for ET nanorods, 3.28 eV for WT nanorods, 3.27 eV for QO nanocrystals. All these band energies are larger than that of 3.1eV previously reported for brookite nanosheets.[24] However, ET nanorods showed a different absorbance between 380 and 420 nm, which should be due to the presence of some defects generated from the adsorption of SO_4^{2-} onto the nanorod surfaces in hydrothermal condition. This is because SO_4^{2-} species has a higher affinity to Ti^{4+} in an aqueous solution relative to many other anions (such as Cl^-, NO_3^-,ClO_3^-, ClO_4^-, or -OOH),[8] which also resulted in the absence of special crystal facet exposed at the tips of the ellipsoid nanorods and a complex of single crystal and polycrtstal (Fig.S3F).

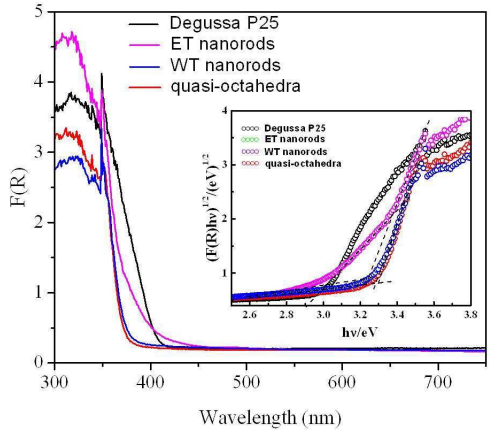

Fig. 3 DRS spectra of the as-prepared brookite with varied shapes and Degussa P25. Insert is the plot of $(h\nu)^{1/2}$ versus energy ($h\nu$).

3.2 Photocatalytic performances of brookite with different shapes

Shape-dependent physicochemical properties arising from different surface energy of nanomaterials have generated more and more interest in the possible applications. The exposure of distinct redox facets can facilitate charge carrier transport to different facets, thereby reducing the charge recombination rate.[31] The chemical nature of these facets was studied through oriented deposition of other species. Here, we performed photo-deposition experiments to identify the redox sites on the facets of brookite QO nanocrystals. It is found that, under UV-light illumination, PbO_2 grains were deposited onto brookite {201} facets (Figs. S4 and S5), somewhat like photocatalytic oxidation deposition of ZnO_2 onto brookite,[6] while Pt nanoparticles (2-3 nm) were mainly loaded onto the planes {210} and {101}. Therefore, we

inferred that facets {201} mainly acted as the oxidative surfaces, while {210} and {101} facets function as the reductive sites. The presence of redox facets of brookite nanocrystals is beneficial for spatial separation of photo-generated electrons and holes between different facets, thus providing the possibilities of improving photocatalytic performances.

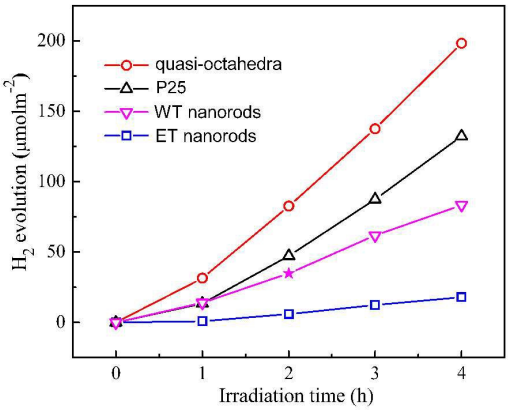

Fig. 4 Normalized hydrogen evolution amounts as a function of irradiation time for brookite nanocrystals with different shapes under light irradiation (780≥λ≥340 nm). The relevant data for Degussa P25 were also given for comparison.

To confirm this assumption, transient photocurrent responses were examined for these brookite particles. As illustrated in Fig. S6, electrodes made of brookite TiO_2 with redox facets (QO and WT nanorods) or heterojunctions (Degussa P25) exhibited efficient separation of the photogenerated carries except for ET nanorods. The quick photocurrent response was beneficial for the synergy of redox facets or heterostructure which facilitated the separation of photogenerated electron and holes. ET brookite TiO_2 nanorods, however, exhibited a negligible photocurrent, which could be due to the presence of defects (Fig. 3) induced by the surface absorbed SO_4^{2-} species in hydrothermal process that causes the recombination of the photoexcited carries.

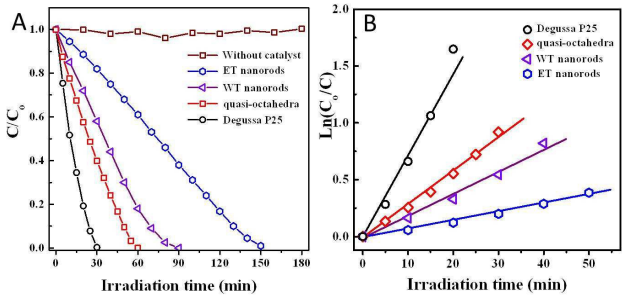

Fig. 5 (A) Photocatalytic activities of brookite nanocrystals with different shapes in MO degradation. The relevant data of Degussa P25 was provided for comparison. (B) The correlative rate constants determination of MO degradation

Generally, catalysts with a lower recombination rate of photo-induced charge carriers will be more reactive in reactions. Based on the photocurrent tests (Fig. S6), separation capabilities of photogenerated electrons and holes for brookite with different shapes were found to follow such a sequence: WT nanorods > QO nanocrystals > ET nanorods. It is well known that photocatalytic reactions are typical of surface-based processes, and hence surface area could be a pivotal factor in determining the apparent performance. For the purpose of more accurate evaluation, reactivity comparisons were carried out after normalization of the BET specific surface areas (Table 1 and Fig.S7). Photocatalytic generation of hydrogen was employed to evaluate the photoreduction activities of these faceted brookite crystals. As shown in Fig. 4, brookite QO nanocrystals exhibited the biggest rate for hydrogen production (~1000 μmoL·m^{-2}·h^{-1}·g^{-1}), about 7 times or 2.5 times higher than that of ET nanorods and WT nanorods, respectively. Furthermore, photocatalytic performances for creating hydrogen over brookite QO nanocrystals was even much better than that of Degussa P25 in spite of its relatively weak power in separating the photoexcited carries. Hence, we could come to the conclusion that photoreactivity of hydrogen evolution for brookite nanocrystals comply with the order of QO nanocrystals > WT nanorods > ET nanorods. In addition, the same activity order was observed for these nanocrystals in photodegradation of methyl orange (MO) organic dyes (Fig. 5). Obviously, a tardy photoactivity displayed in ET nanorods was ascribed to the defects caused by the surface adsorbed SO_4^{2-} in preparation and thus retards the separation of photogenerated carries and decomposition of MO, which is consistent with the lowest photoactivities in water splitting (Fig. 4). Completely breaking down MO needs 90 min for WT nanorods and 60 min for brookite QO nanocrystals. The apparent pseudo-first-order rate was determined according to $ln(C_o/C) = kt$. The obtained k values were listed in Table 1, which reveals a positive correlation with photoreactivities. Therefore, the above experimental outcomes manifest that photocatalytic performance of brookite TiO_2 is highly surface-facets dependent, which can be remarkably heightened through augmentation of the reactive facets {101} and {201}.

3.3 Crystal effects and photocatalytic mechanism of brookite with different shapes

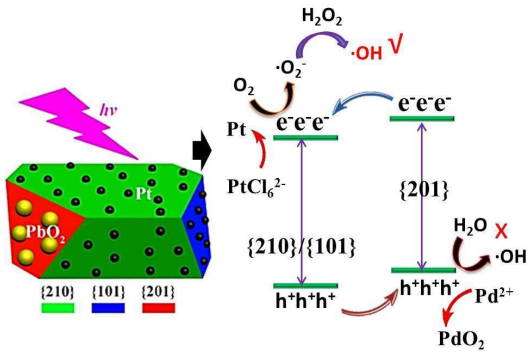

Fig. 6 Mechanism proposed for facet-dependent photoexcited carries transformation and photodeposition of Pt and PbO_2 species onto the redox surfaces of brookite QO nanocrystals.

The observation of unique chemical nature of these facets is surprising. In order to interpret this phenomenon, electronic band structures of brookite nanocrystals with different shapes were investigated by X-ray photoelectron spectra. Although QO nanocrystals possess nearly the same bandgap as that of WT nanorods (Fig. 3), the valence band maximum (VB_{max}) of QO

nanocrystals shifted apparently upwards by 0.18 eV relative to WT nanorods (Fig. S8). Consequently, conduction band minimum (CB_{min}) of QO nanocrystals is raised up. On the other hand, no traces of Ti^{3+} or Ti^{2+} were detected in these samples (Fig. S9). By comparison, the difference of CB_{min} and VB_{max} of brookite just originated from the percentage of oxidative facet {201} and reductive surfaces {210} and {101}. As a result, both CB_{min} and VB_{max} of {201} planes could be higher than those of facets {210} and {101}. Such differences in energy levels can drive holes to move forward to the {201} facets, while electrons to other planes, similar to those reported in other systems,[32-34] accounting for the unique chemical nature of these facets. With these, transformation mechanism of electrons and holes at different planes is proposed and displayed in Fig. 6.

In photocatalysis such as inactivating E. coli[35] and degradation of organic pollutions,[36] $\cdot O_2^-$ and ·OH are well-known active species, which are generated as photogenerated electrons efficiently transfer. Considering the band-gap energy (Fig. 3) and the redox potential of the valence band (VB, Fig. S8) in brookite, $\cdot O_2^-$ production is thermodynamically favored by directly reducing O_2 into $\cdot O_2^-$ [$E^0(O_2/\cdot O_2^-$ = - 0.33 eV *vs* NHE) by CB (more negative than -1.0 eV *vs* NHE) of brookite. Alternatively, ·OH generation is thermodynamically forbidden as its valence band (less than +2.18 eV *vs* NHE) cannot directly oxidize H_2O/OH^- [$E^0(OH/\cdot OH$ = 2.38 eV *vs* NHE)).[35] Even so, ·OH could be generated from the reductive site in brookite by reducing the absorbed oxygen to generate $\cdot O_2^-$. Subsequently, there occurs a facile disproportionation that produces ·OH by a two-electron oxygen reduction route ($\cdot O_2^- + 2H^+ + 2e^- \rightarrow H_2O_2 \rightarrow 2\cdot OH$),[36, 37] as clearly demonstrated in Fig. 6.

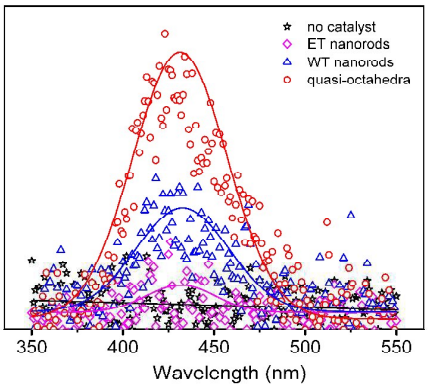

Fig. 7 Fluorescence emission spectra of TAOH produced in the presence of brookite QO nanocrystals, ET nanorods, and WT nanorods under UV irradiation for given period of time.

Here, ·OH radicals produced from catalyst under UV-light irradiation were monitored using terephthalic acid as a trapping agent. Since most photoexcited carries will recombine again, only a small part of the photogenerated electrons can efficiently separate and transfer to the surface of brookite TiO_2, then take part in the photo-reductive actions. Photogenerated electrons were studied indirectly by detecting the production of ·OH radicals, as depicted in Figs. 7 and S10. No signals for ·OH radicals were found at the absence of catalyst, and negligible ·OH radicals were produced in ET nanorods after 9 min UV-light illumination. Comparatively, greatly enhanced ·OH radical signals appeared as WT nanorods and QO nanocrystals were introduced. More importantly, the sequence of the intensity of ·OH radicals is in good agreement with the amount of H_2 production (Fig. 4) and MO degradation (Fig. 5). These observations further demonstrate that brookite nanocrystals with distinct redox facets could facilitate the separation of charge carriers that participate in photoreactions, thus greatly promoting the photocatalytic activity.

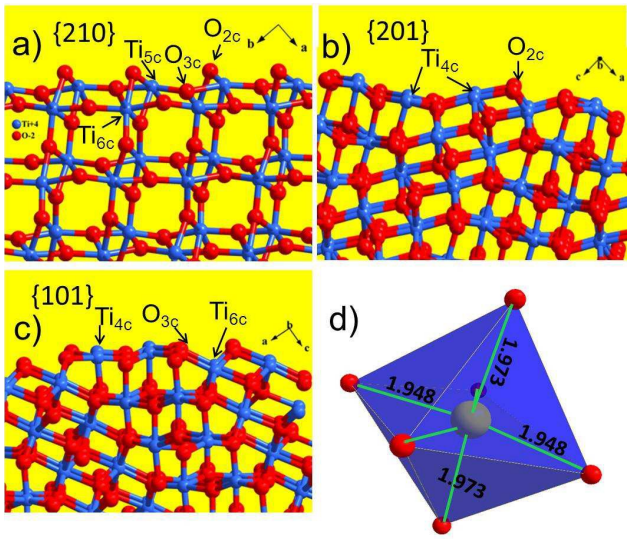

Fig. 8 Ball-and-stick facet model of brookite TiO_2: (a) facet {210}, (b) facet {201}, and (c) facet {101}. O atoms are marked red, and Ti atoms are marked blue. (d) The coordination of the Ti atom located at the centre of TiO_6 octahedra in brookite. The calculated bond distances are given in Å,[38] and O atoms are in red and Ti in grey.

The atomic structures of the exposed facets for brookite may have impacts on catalytic performances. The facet models for brookite are illustrated in Fig. 8. There are coordinatively unsaturated (cus) five-fold Ti (Ti_{5c}) and two-fold O (O_{2c}), as well as saturated six-fold Ti (Ti_{6c}) and three-fold O (O_{3c}) atoms in the {210} surface (Fig. 8a). For {101} plane (Fig. 8b), cus Ti_{4c}, Ti_{5c}, and O_{2c} atoms, along with co-ordinatively saturated Ti_{6c} and O_{3c} atoms were clearly revealed. It appears to be rather striking that, an infrequent high-index {201} facet exposed with cus Ti_{4c}, Ti_{5c}, O_{2c}, together with saturated Ti_{6c} and O_{3c} atoms was cleaved from the brookite lattice (Fig. 8c). Notably, the percentage of Ti_{4c} and Ti_{5c} in {201} is the largest among these facets mentioned above, and {101} exhibits a higher density of unsaturated Ti_{4c} and Ti_{5c} as compared to {210} facets. Theoretical investigations have demonstrated that the surface formation energy of these facets sticks to the following subsequence: 0.62 J/m^2 for {001}, < 0.70 J/m^2 for {210}, and < 0.87 J/m^2 for {101}.[38] Even though the surface energy of {201} has not been disclosed before, we believe that {201} facet could be gifted by a much higher energy than {101} in view of its presence of more cus atoms. Fig. 8d illustrates the TiO_6 octahedra (Ti_{6c}) with the Ti atom at the centre. Notably, six Ti-O bonds are all different in the case of brookite, which is much different from other polymorphs like anatase and rutile.[38]

Moreover, in the production of H_2, the existence of redox facets reveals an efficient spatial separation of the photogenerated electrons and holes between {210} and {201} facets, which are

mainly owing to the different energy levels of these facets.[32, 34, 38] Because of more effective electrons (Fig. 7) generated and the 'surface heterojunction'[33] constructed by the redox facets, it is reasonable that the QO nanocrystals exhibited an excellent photoactivity superior to those of WT and ET nanorods. Additionally, the surface atomic structure also determines the performance of photocatalystic water splitting.[39] As demonstrated in Fig. 6, the percentage of coordinatively unsaturated (Ti-O bond) Ti_{4c} and Ti_{5c} atoms in {201} facet is the largest, while {101} planes exhibit a higher density of cus Ti_{4c} and Ti_{5c} as compared to {210} surfaces. It means that the reduction facets of {210} (amounting up to 70%) in brookite QO nanocrystals possess more Ti-O bonds and expose more oxygen atoms than the oxidation facts {201} and {210}. Eventually, brookite QO nanocrystals exposed with redox facets gifted with both favorable surface atomic and electronic structure can orient the deposition of noble metals, leading to the outstanding activities towards hydrogen evolution and pollutant elimination. This finding may be useful to design and construct novel and highly efficient semiconductors photocatalysts in solar energy conversion and environment applications.

4. Conclusions

Brookite TiO_2 with quasi-octahedra, ellipsoid-tipped and wedge-tipped nanorod has been synthesized through the tailored water-soluble precursors under hydrothermal procedure. The obtained brookite quasi-octahedra nanocrystals with redox facets have shown the highest concentration of photogenerated ·OH and photocatalytic performances for water splitting and MO elimination. These advantages come from the unsaturated coordinative Ti and O atoms in the redox planes, which lowered the charge transfer resistance, reduced the charge recombination, and improved the photocatalytic activity. The low photoactivities of ellipsoid-tipped brookite TiO_2 nanorods were ascribed to the surface adsorbed SO_4^{2-} that results in lots of defects, thus retarding the separation of photogenerated carries. All these demonstrate that redox facets were significant for the improved photocatalytic activity. The precursor-directed synthetic route demonstrated here can be a promising strategy to construct the low-cost and high efficiency metastable and/or functional inorganic nanomaterials with specific facet exposed for environment and energy applications.

Acknowledgements

We acknowledge the NSFC (21401190, 21025104, 21271171 and 91022018) and Science and Technology Programs from Fujian Province (2013H0057) for financial support. The authors thank Prof. Qing-Ping Wu for assistance in the SAED testing.

Notes and references

[a]*Key Laboratory of Design and Assembly of Functional Nanostructures, Fujian Institute of Research on the Structure of Matter, Chinese Academy of Sciences, Fuzhou 350002, P. R. China.*
Fax: (+)86-591-63179431; Tel: (+)86-591-63179431; E-mail: lipingli@fjirsm.ac.cn; guangshe@fjirsm.ac.cn

† Electronic Supplementary Information (ESI) available: [details of any supplementary information available should be included here]. See DOI: 10.1039/b000000x/

1. M. Cargnello, T.R. Gordon, C.B. Murray, *Chem. Rev.*, 2014, **114**, 9319-9345.
2. Y. Bai, I. Mora-Sero, F. De Angelis, J. Bisquert, P. Wang, *Chem. Rev.*, 2014, **114**, 10095-10130.
3. A. Di Paola, M. Bellardita, L. Palmisano, *Catalysts*, 2013, **3**, 36-73.
4. Y.P. Zang, L.P. Li, Y.S. Xu, Y. Zuo, G.S. Li, *J. Mater. Chem. A*, 2014, **2**, 15774-15780.
5. D. Dambournet, I. Belharouak, K. Amine, *Chem. Mater.*, 2010, **22**, 1173-1179.
6. M.C. Guo, L.P. Li, H.F. Lin, Y. Zuo, X.S. Huang, G.S. Li, *Chem. Commun.*, 2013, **49**, 11752-11754.
7. J.L. Xu, K. Li, S.F. Wu, W.Y. Shi, T.Y. Peng, *J. Mater. Chem. A*, 2015, **3**, 7453-7462.
8. J.G. Li, T. Ishigaki, X.D. Sun, *J. Phys. Chem. C*, 2007, **111**, 4969-4976.
9. W.B. Hu, L.P. Li, G.S. Li, Y. Liu, R.L. Withers, *Sci. Rep.*, 2014, **4**. 6582-6590.
10. G.H. Tian, H.G. Fu, L.Q. Jing, B.F. Xin, K. Pan, *J. Phys. Chem. C*, 2008, **112**, 3083-3089.
11. J.C. Yu, L.Z. Zhang, J.G. Yu, *Chem. Mater.*, 2002, **14**, 4647-4653.
12. M.H. Yang, P.C. Chen, M.C. Tsai, T.T. Chen, I.C. Chang, H.T. Chiu, C.Y. Lee, *CrystEngComm*, 2014, **16**, 441-447.
13. Q.X. Deng, M.D. Wei, X.K. Ding, L.L. Jiang, B.H. Ye, K.M. Wei, *Chem. Commun.*, 2008, 3657-3659.
14. T. Nagase, T. Ebina, T. Iwasaki, K. Hayashi, Y. Onodera, M. Chatterjee, *Chem. Lett.*, 1999, 911-912.
15. W.B. Hu, L.P. Li, G.S. Li, C.L. Tang, L. Sun, *Cryst. Growth. Des.*, 2009, **9**, 3676-3682.
16. B. Zhao, F. Chen, Q.W. Huang, J.L. Zhang, *Chem. Commun.*, 2009, 5115-5117.
17. J.Zhao, Y. Liu, M.H. Fan, L. Yuan, X.X. Zou, *Inorg. Chem. Front.*, 2015, **2**, 198-212.
18. Y.S. Xu, W.D. Zhang, *CrystEngComm*, 2013, **15**, 5407-5411.
19. M.Y. Masoomi, A. Morsali, *Coordin. Chem. Rev.*, 2012, **256**, 2921-2943.
20. K. Tomita, V. Petrykin, M. Kobayashi, M. Shiro, M. Yoshimura, M. Kakihana, *Angew. Chem. Int. Edit.*, 2006, **45**, 2378-2381.
21. M. Kobayashi, V.V. Petrykin, M. Kakihana, *Chem. Mater.*, 2007, **19**, 5373-5376.
22. M. Kobayashi, K. Tomita, V. Petrykin, M. Yoshimura, M. Kakihana, *J. Mater. Sci.*, 2008, **43**, 2158-2162.
23. Y. Ohno, K. Tomita, Y. Komatsubara, T. Taniguchi, K. Katsumata, N. Matsushita, T. Kogure, K. Okada, *Cryst. Growth. Des.*, 2011, **11**, 4831-4836.
24. H.F. Lin, L.P. Li, M.L. Zhao, X.S. Huang, X.M. Chen, G.S. Li, R.C. Yu, *J. Am. Chem. Soc.*, 2012, **134**, 8328-8331.
25. A. Pottier, C. Chaneac, E. Tronc, L. Mazerolles, J.P. Jolivet, *J. Mater. Chem*, 2001, **11**, 1116-1121.
26. T.A. Kandiel, A. Feldhoff, L. Robben, R. Dillert, D.W. Bahnemann, *Chem. Mater.*, 2010, **22**, 2050-2060.
27. D. Truong, M. Kobayashi, H. Kato, M. Kakihana, *J. Ceram. Soc. Jpn.*, 2011, **119**, 513-516.
28. R. Buonsanti, V. Grillo, E. Carlino, C. Giannini, T. Kipp, R. Cingolani, P.D. Cozzoli, *J. Am. Chem. Soc.*, 2008, **130**, 11223-11233.
29. K. Katsumata, Y. Ohno, K. Tomita, T. Taniguchi, N. Matsushita, K. Okada, *Acs. Appl. Mater. Inter.*, 2012, **4**, 4846-4852.
30. A. Hagfeldt, M. Gratzel, *Chem. Rev.*, 1995, **95**, 49-68.
31. N. Roy, Y. Sohn, D. Pradhan, *Acs. Nano.*, 2013, **7**, 2532-2540.
32. M. Zhao, H. Xu, H.R. Chen, S.X. Ouyang, N. Umezawa, D.F. Wang, J.H. Ye, *J Mater Chem A*, 2015, **3**, 2331-2337.
33. J.G. Yu, J.X. Low, W. Xiao, P. Zhou, M. Jaroniec, *J. Am. Chem. Soc.*, 2014, **136**, 8839-8842.
34. R.G. Li, F.X. Zhang, D.G. Wang, J.X. Yang, M.R. Li, J. Zhu, X. Zhou, H.X. Han, C. Li, *Nat. Commun.*, 2013, **4**, 1432-1438.
35. D.H. Xia, Z.R. Shen, G.C. Huang, W.J. Wang, J.C. Yu, P.K. Wong, *Environ. Sci. Technol.*, 2015, **49**, 6264-6273.
36. Y.S. Xu, W.D. Zhang, *ChemCatChem*, 2013, **5**, 2343-2351.
37. J. Jiang, H. Li, L.Z. Zhang, *Chem. Eur. J.*, 2012, **18**, 6360-6369.
38. X.Q. Gong, A. Selloni, *Phys. Rev. B*, 2007, **76**, 235307-235317.
39. J. Pan, G. Liu, G.M. Lu, H.M. Cheng, *Angew. Chem. Int. Edit.*, 2011, **50**, 2133-2137.

A table of contents entry

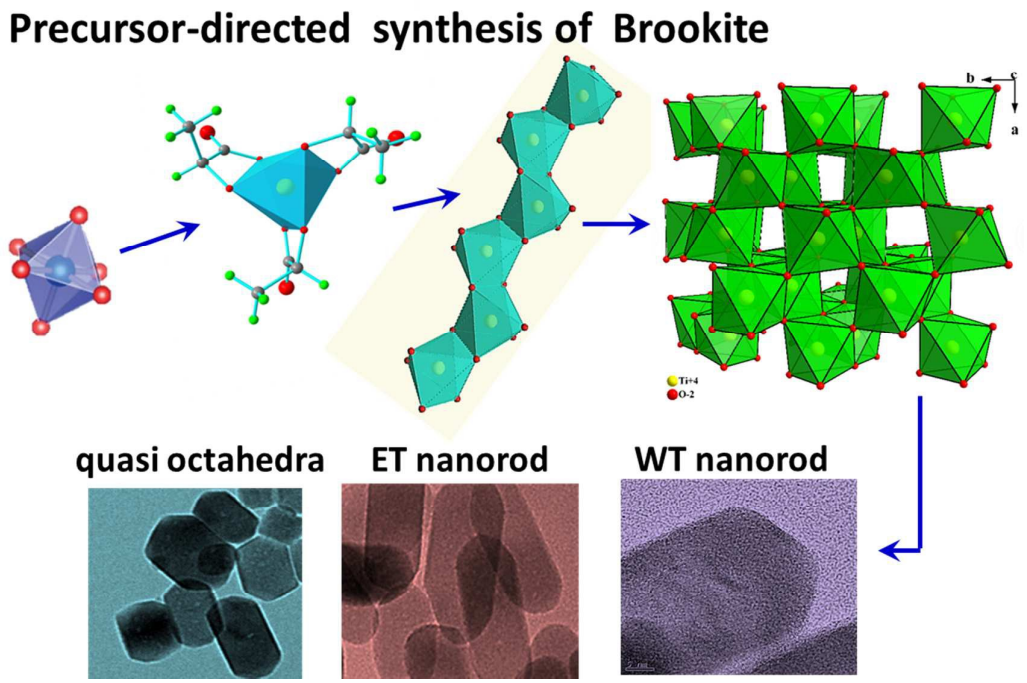

Quasi octahedral, ellipsoid-tipped and wedge-tipped nanorods Brookite TiO_2 were tailored and synthesized via water-soluble titanium precursor directed strategy.